Mechanical Design and Optimization of a Micro-surgical Robot

Mathieu Miroir, Jerome Szewczyk, Olivier Sterkers, Yann Nguyen and Stéphane Mazalaigue

***Abstract*— A tele-operated system with three arms for the middle ear micro surgery is presented. It is composed of an operator console from where the surgeon tele-operates all of three robotised arms carrying for each one a surgery tool holder with a high level of accuracy. The specificity and advantage of these micro-manipulators compared to existing robots dedicated to mini-invasive surgery are an increased field of vision and an increased capacity to carry out complex operational gestures without using dextral tool with intra-body mobility. The method used to design the micromanipulator tool holder is described. A first task consists in analysing functional specifications. The next step is to define and select a kinematic structure adapted to the task. Finally, a dimensional optimization is carried out by using Pareto front method.**

I. INTRODUCTION

For more than ten years, important developments in robotised minimal invasive surgery have been carried out in the fields of laparoscopy [1] or cardiac surgery [2] for example. The goal is to improve the precision, the safety of the gesture and the comfort of the surgeon.

On the contrary, the robotic assistance to microsurgery is a recent research domain with many potential applications in the fields of neurosurgery [3], ophthalmology [4] or ENT (Ear Nose Throat) [5] [6] surgery. In this case, the design of a robotic assistance system has to face specific problems and at the present time, no robotised device dedicated to the micro-surgery is used in a clinical context.

Our main objective is thus to develop a robotised system for the micro-surgery and especially the middle ear surgery (see Fig. 1). Different robotic systems have already been developed and dedicated to this surgery [7], [8] and [9]. However, these systems do not fully satisfy all the task requirements and in particular the problems of overall size limitation and fabrication costs minimization. Our approach will take into account all the technical constraints related to this particular kind of intervention. Moreover, economic and technological requirements inherent to every industrial product will be considered.

In this paper, we first describe the concerned surgical application and characterize the tasks devoted to the controlled device. The choice and the optimal dimensioning of a kinematic structure and of the actuators are then presented. Finally, geometrical parameters of the chosen structure are optimized in regards to the specifications.

This work was supported by Collin ORL Inc, Bagneux, France and Hopital Beaujon ENT departement AP-HP, Paris, France

M. Miroir is with Faculty of Pierre et Marie Curie, Paris, France and with company Collin Inc, Bagneux, France miroir@isir.fr

J. Szewczyk is with Faculty of Pierre et Marie Curie, Paris, France szewczyck@isir.fr

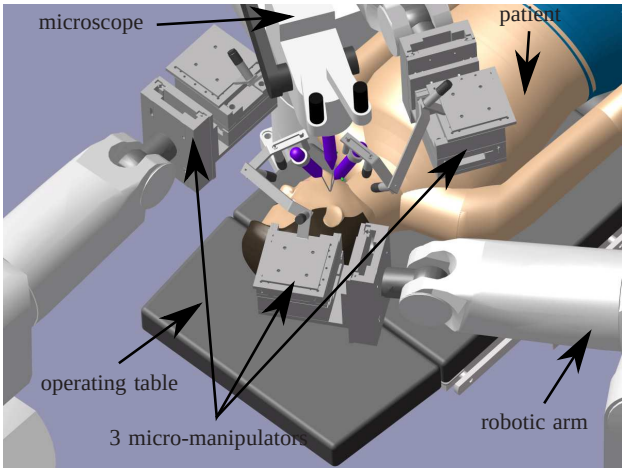

Fig. 1. Overview of a possible assistance robot for the middle ear surgery

II. DESIGN SPECIFICATIONS

The envisaged system must be able to carry out surgery in the middle ear (see Fig 2) like those actually performed on the micro-surgical treatment of the otosclerosis. The path usually used to insert the instruments into the middle ear is through the external ear after raising a tympanomeatal flap [10], [11]. The patient's head is oriented on side and immobilized. The surgeon can observe the operation area only through a microscope placed at the vertical of the external ear canal at a maximum of 30 cm. The tools is introduced into the patient's ear through a funnel shape speculum (see figure 2).

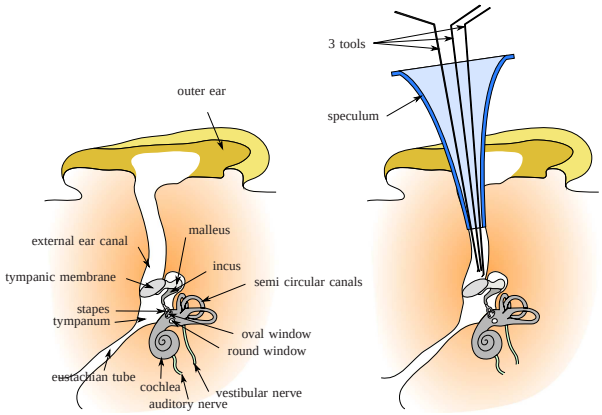

Fig. 2. Human ear with speculum and 3 tools

Usually, two tools must be introduced at the same time into operating field. The surgeon is then constrained to handle one

of while holding the speculum to maintain his field of view. Moreover, an additional suction pipe is permanently in the operation field. This pipe can not be removed as it evacuates the blood outside the operation area.

Under these conditions, the system which has to be developed will include three mandatory micro-manipulators.

Each one is dedicated to the manipulation of a surgical tool. These micro-manipulators will have to be sufficiently compact to take place near the ear operated without being in contact with the microscope. They will be carried by three standard robotised arms used for high displacements. Figure 1 illustrates the global view of the system. The surgeon tele-operates the unit using a remote device.

III. EXPECTED PERFORMANCES

In the following, the performances expected for the systems' micro-manipulators will be detailed.

A. Internal workspace

The workspace associated with the task that has to be robotised includes :

- firstly in terms of reachable spacefield: a volume made up of the external auditory canal, scutum lowering, visible part of the tympanum,
- secondly: all the reachable orientations by a rectilinear tool introduced into this volume (see figure 3).

The goal is to modelize these volumes in order to take into account all morphologies and thus to ensure the possibility of being able to treat the most people. Therefore, a great panel of people had to be tested.

With the assistance of the surgeons, the morphology of several patients was thus measured on temporal bone CT-Scan images in order to obtain for each one dimensions of the smallest cylinder including volume described above. After a first selection, 20 different morphologies were analysed. The largest diameter and the highest cylinder obtained are given on figure 3. This cylinder of reference is added to a truncated cone materializing the speculum introduction in order to define the workspace.

The morphological statements were obtained thanks to the Digipointeur® that is a navigation system created and marketed by the company Collin ORL Inc [12]. It allows to reconsctruct a three dimensional model of all the needed anatomic structures volumes from CT Scan images of a patient head in axial planes. Moreover, it allows the measurement in any plan in 2D as well as measurements in 3D. The bottom of the figure 3 shows the Digipointeur® screen. At the top to the left the user can navigate in the patient's radiography in axial planes. At the top right are displayed coronal planes. On the right below sagittal planes are represented. In the left inferior corner are indicated the results of the realized measures.

The diameter of the cylinder was measured on the sagittal planes reconstructions. The height of the cylinder was obtained by measuring the distance between the beginning of the auditory canal in the axial plan (origin point on this figure) to the deepest region of the operating field

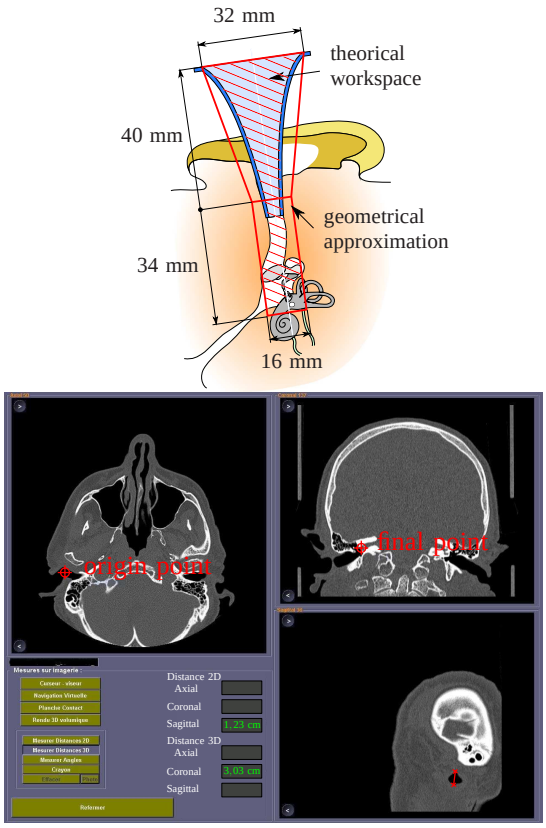

Fig. 3. geometrical measurement and approximation of the workspace

corresponding to the oval window in the coronal plan (final point on this figure).

B. Tool/organ forces measurements

Within the framework of a surgical operation for the treatment of the otosclerosis, the interactions tool/organ leading to significant efforts of contact are: lowering of the scutum using a drill or a curette (see figure 4), stapedial tendon section, posterior and anterior crura of the stapes section (see figure 5), incudo stapedial joint separation (see figure 6)),stapes superstructure removal, stapedotomy [13] (drilling and sizing of the stapes footplate fenestration figure 7), prosthesis positioning and crimping (see figure 8).

In order to measure these efforts, the test bench of figure 9 was used. It allows to reproduce the gestures of the surgical steps on fresh temporal bone anatomic specimen. One can measure the efforts of interaction between tool and organ using a force sensor ATI nano 43 (with a resolution equal to 1/512 N and 1/40 N.mm) placed under the box containing the temporal bone.

Each gesture was measured 10 times in order to ensure repetability and several types of tools were tested and two surgeons (a junior and a senior) were solicited. The results obtained are gathered in table I. The minimal, maximal forces and those selected for every gesture are referenced there. The selected results correspond to the effort which seems necessary to bring to do successful the gesture even if a time increment is necessary.

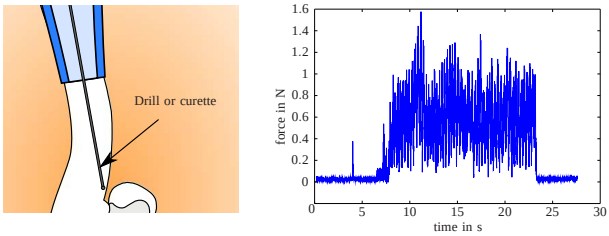

Fig. 4. Scutum lowering

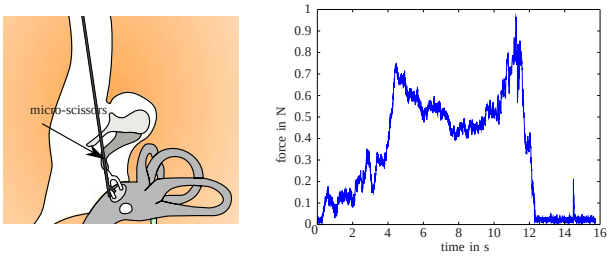

Fig. 5. section of the stapes posterior crura

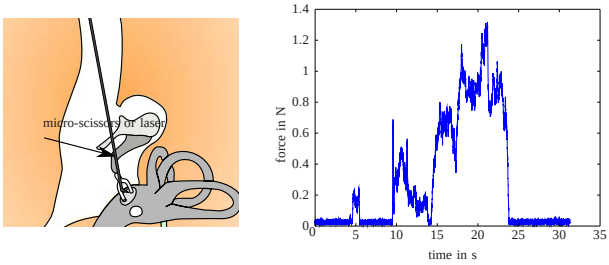

Fig. 6. section of the stapes anterior crura

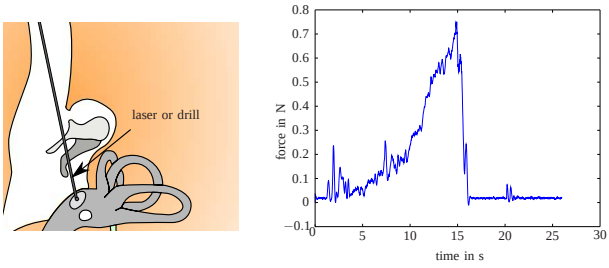

Fig. 7. stapedotomy

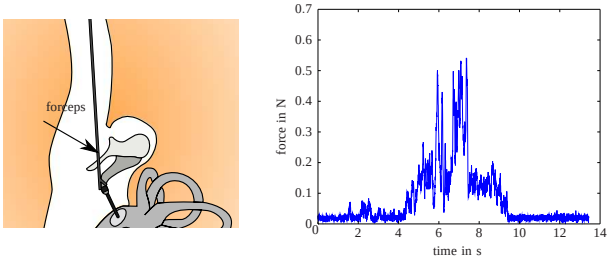

Fig. 8. prosthesis crimping

C. Precision and resolution

Among the gestures described in the previous paragraph, the drilling of the footplate is the one requiring the highest precision. The hole must be located exactly under the incus and has to be as round shaped as possible.

The surgeons consider acceptable a positioning error of the drilling center and a circularity error not exceeding 1 % of the diameter of the piston to be inserted (figure 10). This corresponds, for a theoretical pitch circle diameter of 0,5 mm, to a precision of linear positioning of the tool of 5 µm and with a angular positioning precision of 8 °.

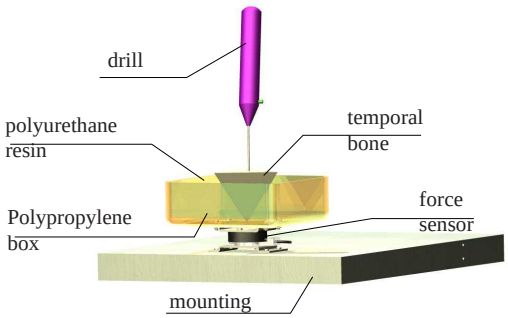

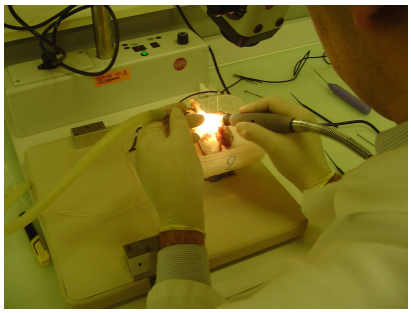

Fig. 9. experimental setup for measuring the forces

TABLE I
SUMMARY OF FORCES GESTURES CARRIED OUT DURING THE OTOSCLEROSIS

practised gesture	minimal forces	maximal forces	selected forces
scutum lowering performed with low speed drill 10000 RPM	1.6 N	4.25 N	2 N
scutum lowering performed with high speed drill 30000 RPM	2.5 N	3.5 N	3 N
scutum curetting by surgeon hand	7 N	20 N	
tendon section	0.45 N	1 N	0.7 N
posterior crura section	0.9 N	1.8 N	1.2 N
incudostapedial joint separation	0.7 N	2.75 N	1.5 N
anterior crura section	0.8 N	1.6 N	1.2 N
stapedotomy	0.75 N	1.5 N	1.25 N

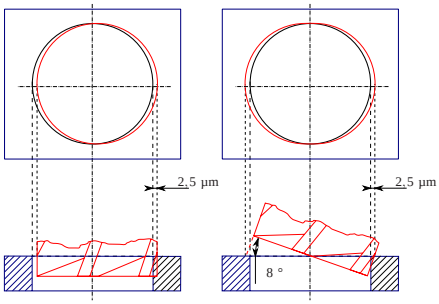

Fig. 10. awaiting resolution

The system has tele-operation capabilities using indirect visual feedback to the surgeon. Under these conditions, the

precision of positioning of the tool depends only on the image quality and on the resolution of the micromanipulator. It will have to thus be at least equal to a resolution of 5 µm in translations and a resolution of 8 ° in rotations.

This second constraint is satisfied a priori without difficulty. On the other hand, the linear constraint of 5 µm resolution will strongly condition the choice of a motorization for the developed micromanipulator. For example, let us consider a tool carried out by a high quality industrial manipulator such as a Staübli TX40. If the length of the tool is equal to 15 cm then the precision of the tip can exceed 25 µm. The main reason is that the angular resolution of the last axis is higher than $0,172.10^{-3}$ °.

D. External workspace

Figure 11 shows the constraint of obstruction caused by the body of the patient and the presence within 30 cm of the microscope. In green on this figure, we represented the field of vision of the microscope. It must be as large as possible during the operation.

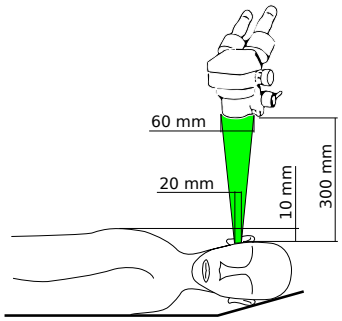

Fig. 11. a global view of the intervention environment

IV. TOPOLOGIC STRUCTURE

A. Kinematics selection

Fig. 12, 13, 14 and 15 show four candidate kinematic structures. These structures are kinematically non-redundant in order to minimize the complexity and costs. All these structures are mounted on Cartesian "cross tables" in order to decouple translations from rotations of the tool. Moreover, the large displacements along the speculum axis can be entirely supported by the Z-axis of the cross table. In the same way, the four structures have a final rotoid joint devoted to perform large rotations around the tool axis.

The kinematics of Fig. 12 is a classical serial structure finished by a convergent wrist with orthogonal axes. This kind of structure is relatively simple to conceive and to control. However, it presents the disadvantage of a rotation centre outside the specified workspace. That implies translations on the cross table for pure rotation motion around the tip of the tool.

The kinematics of Fig. 13 has a standard parallel platform well suited to achieve linear and angular displacements with high accuracy. However, the overall size, weight and complexity are prohibiting for the targeted application and it does not have a rotation centre in the workspace either.

The kinematics of Fig. 14 has a rotation centre located at the intersection of the three last rotations axis. A clever choice of these axes allows the centre of rotation to coincide perfectly with the end of the handled tool.

The kinematics of Fig. 15 also carries out an offset rotation centre by means of a motorized parallelogram (mechanism of Evans). Moreover, it allows an increased rigidity and thereby a higher accuracy. However, this kinematics leads to a higher complexity compared to the previous one and the height of the structure is not compatible with the microscope observation.

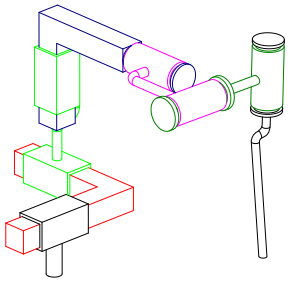

Fig. 12. 6 dof series

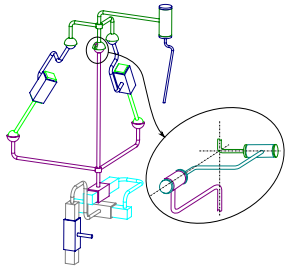

Fig. 13. 6 dof mixed

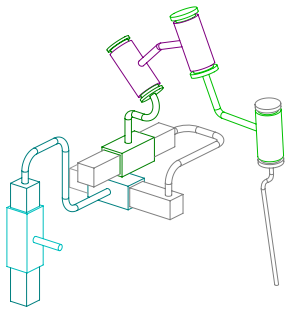

Fig. 14. 6 dof series with offset rotation centre

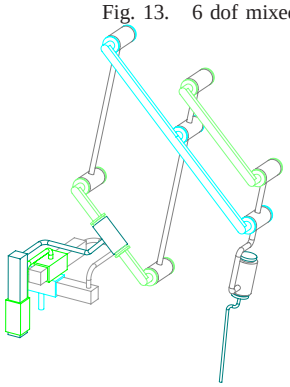

Fig. 15. 6 dof Evans with offset rotation centre

In conclusion of this qualitative analysis of kinematics candidates, the design of the micro-manipulators will be based on the structure presented on the Fig. 14.

B. Actuators

Fig. 16 shows the selected kinematic structure with its motorized joints.

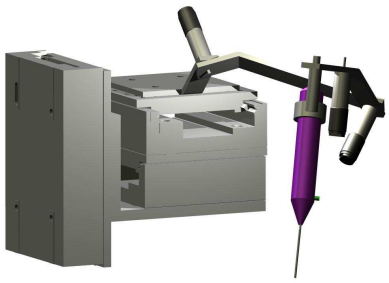

Fig. 16. equipped kinematics

The actuators of the cross table are Newport linear motors which provide very good stroke/size ratio. The first two actuators have a stroke of 25 mm and the third a stroke of 100 mm. The rotation actuators used for the three rotoid links are Faulhaber coreless DC motors selected by their good weight/power ratio.

These actuators guarantee a sufficient displacement resolution at the tip of the tool in regard to the specifications. Indeed, if d is the axial resolution of the cross table motors, we know that the resolution in linear displacement at the tool tip dmax is such that $d_{max} < \sqrt{3}d$. If d = 2 µm (as specified by the manufacturer) then $d_{max} = 3,5$ µm which is lower than the desired resolution $d_{des} = 5$ µm. On the other hand, if q is the angular resolution of the chosen rotation actuators, we know that the resolution in angular displacement of the tool qmax will never be larger than $3q$. Then, if $q = 0,2.10^{-3}$ ° (as specified by the manufacturer) we will have $qmax = 0,6.10^{-3}$ ° which is much lower than $q_{des} = 1$ °.

V. Topological optimization

Fig. 17 shows the joint parameters of the kinematic structure. Five parameters relate to the position of the cross table and are imposed by the dimensions of the chosen linear motors. The other six parameters (Table II) relate to the position of the three rotoid joints and the relevant dimensions of the manipulator.

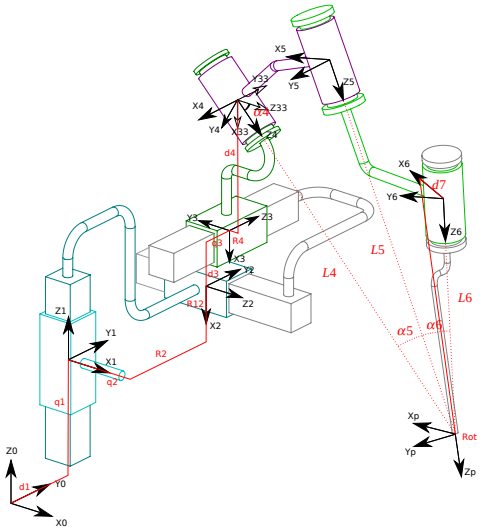

Fig. 17. parameters definition

TABLE II

PARAMETERS VALUES RELATED TO PIVOTS AND DIMENSIONS

	$\alpha 4$	$L5$	$\alpha 5$	$\alpha 6$	$d7$	$L6$
mini values	25 °	90mm	25 °	15 °	5mm	130mm
maxi values	55 °	140mm	60 °	60 °	25mm	180mm
pitch	5 °	10mm	5 °	5 °	5mm	10mm

The values of these remaining geometrical parameters were optimized with respect to the requirements that have not been taken into account at this stage:

- ability to apply desired forces
- distance to the obstacles
- shadow projection of the vision field

The performances of the 90472 manipulators corresponding to the 90472 sets of parameters indicated in Table II were evaluated using a numerical simulation. This simulation consists in calculating all the successive configurations reached by the manipulator when the tool performs a specific 6D trajectory.

This trajectory includes an approach path from an initial reference position and an operative path representative of the workspace in terms of angular and linear displacements. During this trajectory, the upper surface of the cylinder is swept by the end of the tool (see Fig. 18) in 30 steps: 17 for the circle and 13 for the spiral. For each step, the capacity of the robot to produce the maximum slopes of its tool is evaluated in 9 steps. Finally, for each configuration, the capacity of the manipulator to perform a rotation of the tool along its own axis is evaluated with 9 steps.

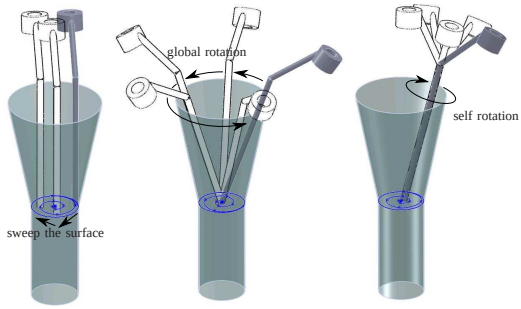

Fig. 18. tool representative trajectory used for the optimization process

As rotation and translations are decoupled, it must be pointed out that the accessibility to the other points of the cylinder does not need to be evaluated. Remarkably, the vertical axis of the robot has a sufficient stroke in comparison with the depth of the workspace. The trajectory thus generated is made up of 2433 configurations ([[17+13]*9*9] +3) including 3 for the approach of the tool. For each reached configuration, the simulation computes:

- the forces that the manipulator can apply at the tool tip
- the smallest distance robot/environment
- the field of vision percentage of the microscope not intercepted by the arm of the robot
- the stroke imposed to the joint actuators

Finally, only 4063 candidate manipulators were able to perform the entire trajectory without contacting the environment or going beyond their joints limits and to produce at each step of the trajectory the required tool tip forces without exceeding their motors capacities.

Each retained manipulator is represented on Fig. 19 by a point positioned according to its scores in terms of smallest distance to the environment during the trajectory and average percentage of non-obstructed vision.

A Pareto's front made up of eleven not-lower solutions [14], [15] can be highlighted on this graph. This Pareto's

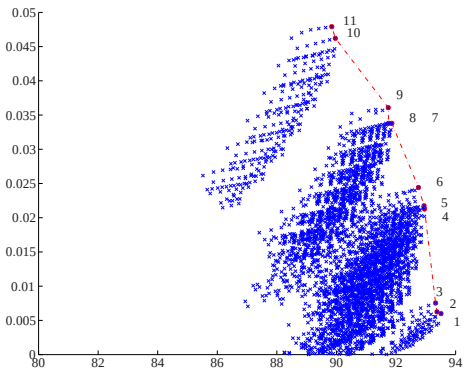

Fig. 19. acceptable configurations plotted in the space minimum distance to the environment vs. the average percentage of vision

TABLE III

END VALUES FOR THE ELEVEN POSSIBLE SOLUTIONS

$\alpha 4$ (°)	$L5$ (mm)	$\alpha 5$ (°)	$\alpha 6$ (°)	$d7$ (mm)	$L6$ (mm)	vision (%)	distance (mm)
30	140	60	50	10	180	93,5	6
50	140	50	50	10	180	93,5	6,2
40	140	40	50	10	180	93,3	7,5
40	140	55	45	5	180	92,9	21,3
50	140	45	45	5	180	92,9	21,7
50	140	40	45	5	180	92,7	24,4
35	140	55	40	5	180	91,8	33,8
50	140	40	40	5	180	91,7	33,8
55	140	40	40	5	180	91,7	36,1
35	140	55	35	5	180	89,9	46,2
55	140	35	35	5	180	89,8	47,9

front has the characteristics to be nearly vertical, all the scores in vision lying between 90 % and 93.5 %.

Logically, we selected the manipulator presenting the best score in terms of distance to the environment. Table III presents the geometrical parameters of the eleven non-lower solutions. The last row corresponds to the selected configuration.

VI. CONCLUSION AND FUTURE WORKS

This paper presents a detailed approach for the design of a robotic system in the field of micro-surgery. It led to a multi-criteria optimization problem resolution in which constraints such as precision and compactness were taken into account. The implemented optimization method is based on a systematic exploration of the parameters domain and a MatLab routine for the constraint evaluations. At this stage, the robot is entirely defined in its geometry and motorization. Future work concern realization and performances test with the help of our clinical partners.

REFERENCES

[1] Akhil J. Madhani, Günter Niemeyer, and J. Kenneth Salisbury, Jr, "The Black Falcon : a Teleoperated Surgical Instrument for Minimally Invasive Surgery", *In Proceedings of the 1998 IEEE/RSJ International Conference on Intelligent Robots and Systems*, volume 2, pages 936–944, Victoria, BC, Canada, 1998.

[2] N. Zemiti and al "Mechatronic Design of a New Robot for Force Control in Minimally Invasive Surgery", *IEEE/ASME Transactions on Mechatronics*, vol 12(2), april 2007,pp 143-153.

[3] P. Di Donato and al "La neuronavigation : principe et intérêt", ITBM-RBM 2000, 21:70-7.

[4] Natalie Smith-Guerin, "Contribution à l'aide robotisée au geste chirurgical ; nouvelle approche en ophtalmologie", PhD thesis, Laboratoire d'Automatique Industrielle de l'INSA de Lyon, 2000.

[5] Russell H. Taylor and al "A Steady-Hand Robotic System for Microsurgical Augmentation", *In MIC- CAI '99 : Proceedings of the Second International Conference on Medical Image Computing and Computer-Assisted Intervention*, pages 1031–1041, London, UK, 1999. Springer-Verlag.

[6] Daniel L. Rothbaum and al "Robot-Assisted Stapedotomy Micropick Fenestration of the Stapes Footplate", *Otolaryngology Head & Neck Surgery Journal*, vol. 127(5), 2002, pp 417-426.

[7] Peter J. Berkelman and al "Performance Evaluation of a Cooperative Manipulation Microsurgical Assistant Robot Applied to Stapedotomy",*In MICCAI '01 : Proceedings of the 4th International Conference on Medical Image Computing and Computer-Assisted Intervention*, pages 1426–1429, London, UK, 2001. Springer-Verlag.

[8] C.-C. Ngan and al "Hexapod-based cochleostomyhexapod basierte cochleostomie", http://www.curac.org/curac06/download/abstracts/18.pdf.

[9] M. Leinung and al "Robotic-guided minimally-invasive cochleostomy: first results", *In: GMS Current Topics in Computer- and Robot-Assisted Surgery (GMS CURAC)*, Vol. 2, No. 1, 2007.

[10] J. Schlosser, "L'Otospongiose", Résonnances, vol. 14, 2004, pp 9-11.

[11] Pierre Elbaz and al "L'Otospongiose", Fondation Adolphe de Rothschild, Paris, 2000.

[12] Collin ORL Inc, Fabricant et Distributeur de matériel pour l'ORL et la Chirurgie Maxillo-Faciale, www.collin-orl.com.

[13] Daniel L. Rothbaum and al "Robot-Assisted Stapedotomy Micropick Fenestration of the Stapes Footplate",*Otolaryngology Head & Neck Surgery Journal*, 127(5), 2002, pp 417-426.

[14] K. Deb and al, "A fast and elitist multi-objective genetic algorithm : NSGA-II", *In: IEEE TRANSACTIONS ON EVOLUTIONARY COMPUTATION*, Vol. 6, No. 2, april 2002.

[15] D. Sallé, "Conception Optimale d'Instruments Robotisés à Haute-Mobilité pour la Chirurgie Mini-Invasive", PhD thesis, Université Pierre et Marie Curie, Paris 6, 2004.